Extending the Relay Feedback Experiment

Soltesz, Kristian; Hägglund, Tore

Published in:
IFAC Proceedings Volumes

DOI:
10.3182/20110828-6-IT-1002.00066

2011

Document Version:
Peer reviewed version (aka post-print)

Extending the Relay Feedback Experiment

Kristian Soltesz * **Tore Hägglund** *

* *Department of Automatic Control, Lund University, Sweden; e-mail:* {*kristian.soltesz, tore.hagglund*}*@control.lth.se*

Abstract: An augmented version of the traditional relay feedback experiment is proposed. It aims at producing an input with energy concentrated to a frequency band, corresponding to a certain phase sector of the Nyquist curve of the process to be identified. A non-convex problem is formulated. Sub-optimal, but efficient, algorithms are developed.

1. INTRODUCTION

1.1 The Role of the Input Spectrum

When performing frequency domain system identification, it is well-known that higher spectral content (magnitude) of a certain frequency in the input generally yields better model accuracy of the obtained model around that frequency. To motivate this, consider estimation of LTI parameters $\boldsymbol{\theta} = [\boldsymbol{b}\ \boldsymbol{a}\ L]^T$ ($\boldsymbol{a} \in \mathbb{R}^n,\ \boldsymbol{b} \in \mathbb{R}^n, L \in \mathbb{R}_+$) of the strictly proper continuous time transfer function process model

$$P(s) = \frac{B(s)}{A(s)} e^{-Ls} = \frac{\sum_{j=1}^{n} b_j s^{n-j}}{s^n + \sum_{i=1}^{n} a_i s^{n-i}} e^{-Ls}, \qquad (1)$$

from sampled input and output data $u(kh),\ y(kh),\ k = 0, \ldots, N-1$, where h is the sampling period. One identification method, presented in Soltesz et al. [2010], is the minimization of the squared output error

$$J(\hat{\boldsymbol{\theta}}) = \frac{1}{2} \int_{t_0}^{t_f} (\hat{y}(t) - y(t))^2 dt, \qquad (2)$$

where y is the output of P generated by u while $\hat{y}$ is the corresponding output of the model $\hat{P}$. The sampled equivalent of (2) is given by

$$J_h(\hat{\boldsymbol{\theta}}) = \frac{1}{2} \sum_{j=0}^{N-1} (\hat{y}(kh) - y(kh))^2. \qquad (3)$$

By Parseval's theorem, applied to the DFT of $\hat{y} - y$, (3) is equivalent to

$$J_h(\hat{\boldsymbol{\theta}}) = \frac{1}{2} \sum_{j=0}^{N-1} |\Delta P(\omega_j)|^2 |U(\omega_j)|^2, \qquad (4)$$

where $\Delta P(\omega) = \hat{P}(i\omega) - P(i\omega)$, U is the N-point DFT of u and $\omega_j = \frac{2\pi}{Nh} j$.

From (4) it can be readily seen that the cost component associated with a certain frequency is proportional to the input power of that frequency. It is therefore natural to ask what input spectrum should be chosen and how to synthesize the corresponding signal in the time domain.

⋆ This work was supported in part by PICLU, the Process Industrial Centre at Lund University.

This paper addresses these questions in the context of system identification for PID tuning.

1.2 Input Spectrum for PID Tuning

The herein described input signal generation is intended to be the first link in a PID auto-tuning tool chain, outlined in Fig. 1.

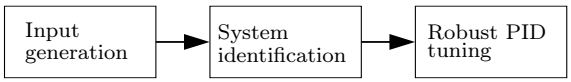

Fig. 1. PID auto-tuning tool chain.

Fig. 2 shows the Nyquist curve of a low pass, time delayed, process typical to process industry. The tuning of a PID controller can be interpreted as moving points of the process Nyquist curve by means of the P, I and D parts, according to the labeled arrows in Fig. 2, cf. Åström and Hägglund [2006].

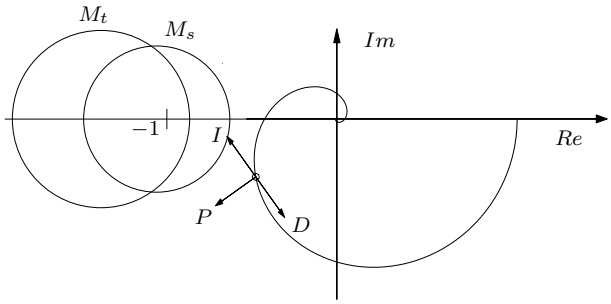

Fig. 2. Nyquist curve interpretation of robust PID tuning.

Conventional methods for robust PID tuning, such as Hägglund and Åström [2002] and Garpinger and Hägglund [2008], ensure robustness by keeping the open loop transfer function outside a region surrounding -1. Avoiding the interior of the circles in Fig. 2 ensures sensitivity $||S||_\infty < M_s$ and complementary sensitivity $||T||_\infty < M_t$.

Both the I and D parts introduce 90° phase shifts (in opposite directions). Hence it is desirable to have accurate models in different frequency regions, depending on which subclass of PID controller is synthesized. E.g., the model

should be accurate around the negative real axis for P controllers, in the third quadrant for PI controllers and in the union of the second and third quadrant for PID controllers.

In this paper we will focus on the PI case, which is the industrially most common. The method can, however, be used for any combination of P, I and D. Hence, we seek an identification input with energy content concentrated to frequencies corresponding to the phase interval $(-180°, -90°)$ of the process to be identified.

1.3 The Use of Relay Feedback

In Åström et al. [1995], it is concluded that stable, well damped LTI systems generally result in stable limit cycle oscillations, under relay feedback. A complete analysis for FOTD (first order plus time delay) systems is given in Lin et al. [2004]. According to describing function analysis, the fundamental harmonic of the oscillation occurs at the frequency ω_{180}, corresponding to the phase $\varphi = -180°$ of the LTI system. This motivated the original relay feedback tuning method, Åström and Hägglund [1984]. Fig. 3(a) shows the experimental setup, with process P and nonlinearity $N.L.$ Fig. 3(b) shows the input signal $u_{a,180}$, corresponding to 6 switches of the relay, with

$$P(s) = \frac{1}{(s+1)(s+2)}e^{-s}. \tag{5}$$

The corresponding power spectrum, plotted against the phase frequencies of (5) is shown in Fig. 3(c). The vertical lines mark the frequencies corresponding to $\varphi = -180°$ and $\varphi = -90°$.

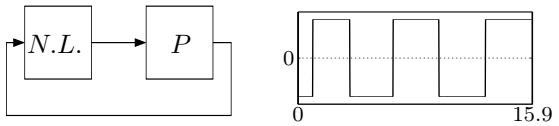

(a) Experimental setup. (b) Input signal $u_{a,180}$ over time [s].

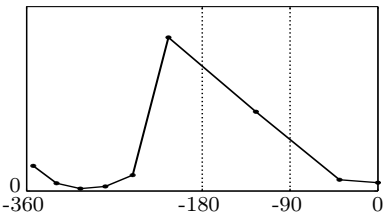

(c) Input power spectrum $|U_{a,180}|^2$ over process phase φ [°].

Fig. 3. Traditional relay experiment and corresponding input power spectrum.

As expected, energy is concentrated around $\varphi = -180°$, rather than distributed over $(-180°, -90°)$, which would be desirable.

By introducing an integrator in the loop, the oscillation frequency is shifted to $\varphi = -90°$, ω_{90}. Fig. 4 shows a nonlinearity described in Friman and Waller [1997], with describing function

$$N(a) = \frac{4h_p}{\pi a} - \frac{4h_i}{\pi a}i, \tag{6}$$

corresponding to limit cycle oscillations at

$$\varphi = \arctan\left(\frac{h_i}{h_p}\right). \tag{7}$$

It may be used to shift the energy peak, but does not address the issue of energy distribution over a frequency interval.

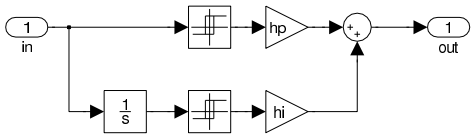

Fig. 4. Two channel relay (Simulink implementation).

2. PROBLEM FORMULATION AND APPROACH

We will now present the input design problem and investigate some approaches. The notation, used throughout the remainder of the paper, is introduced below.

2.1 Notation

Denote by $U \triangleq Fu$ the DFT of u and by $U_j,\ j \in [0, \ldots, N-1]$ its j^{th} component. The DFT matrix F is defined through

$$F_{k,l} = \omega^{kl},\ \omega = e^{\frac{-2\pi i}{N}}. \tag{8}$$

Let

$$\omega_j = \frac{2\pi}{Nh}j,\ a_j = |U_j|,\ P_j = |U_j|^2,\ \phi_j = \angle U_j \tag{9}$$

be the corresponding angular frequency, amplitude, power and phase respectively.

The sample operator associated with sample period h is

$$\text{Ш}_h(t) = \sum_{k=-\infty}^{\infty} \delta(t - kh). \tag{10}$$

2.2 Two Stage Experiment

The aim is to obtain a power spectrum similar to that of Fig. 5 by extending the experiment of Fig. 3(a), while keeping experiment duration short and input power low.

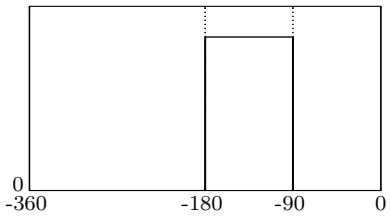

Fig. 5. Reference input power spectrum Q over process phase φ [°].

A first step in this direction is obtained by conducting a two stage experiment, using the two channel relay. Stage one, yielding $u_{a,180}$, shown in Fig. 3(b), consists in 6 switches with $h_p = 1,\ h_i = 0$ $(\varphi = -180°)$. Stage two, yielding $u_{a,90}$, consists in 4 switches with $h_p = 0,\ h_i = 1$ $(\varphi = -90°)$ and is shown together with $u_{a,180}$ in Fig. 6(a). The number of switches were empirically decided, based

on experiments with P, commonly occurring in process industry and listed in Hägglund and Åström [2002]. In order to find the peak frequencies, the two sequences are individually normalized with respect to energy, forming

$$u'_a = \left[\frac{u_{a,180}}{u_{a,180}^T u_{a,180}} \quad \frac{u_{a,90}}{u_{a,90}^T u_{a,90}} \right]^T . \tag{11}$$

The power spectrum $|U'_a|^2$ is shown in Fig. 6(b). Two

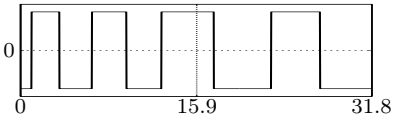

(a) Input signal u_a over time [s].

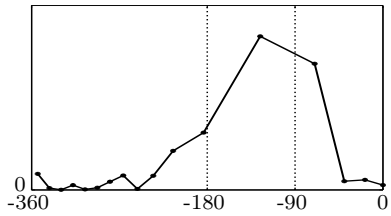

(b) Power spectrum $|U'_a|^2$ over process phase φ [°].

Fig. 6. Two stage relay experiment and corresponding (modified) input power spectrum.

distinct peaks lie close to the frequencies corresponding to the desired phase angles. Experiments show that this is generally true for FOTD and SOTD (second order plus time delay) processes, which is indicated by results presented later in the paper.

The final stage consists in augmenting the experiment in order to obtain a magnitude spectrum similar to that of Fig. 5.

2.3 General Signal Augmentation Problem

An initial experiment has provided a zero order hold input sequence $u_a = [u_{a,180}^T \; u_{a,90}^T]^T$ with sample period h and length N_a, as shown in Fig. 6(a). Using the power spectrum $|U'_A|^2$, the desired power spectrum Q, shown in Fig. 5, can be determined and approached by augmenting u_a with u_b, forming

$$u = \begin{bmatrix} u_a \\ u_b \end{bmatrix}. \tag{12}$$

Assuming fixed length N_b of u_b, we can formulate the synthesis problem

$$\min_{u_b} \underbrace{\left\| Q - \operatorname{diag}\left(F \begin{bmatrix} u_a \\ u_b \end{bmatrix} \begin{bmatrix} u_a \\ u_b \end{bmatrix}^T F^* \right) \right\|_R}_{J(u)}, \tag{13}$$

where R is some vector norm. It is also natural to impose

$$||u_b||_\infty \leq ||u_a||_\infty. \tag{14}$$

The problem, given by (13) is generally not convex in u_b, which can be deduced from e.g. the setup $N_a = 0,\ N_b = 2, u_b = [\, u_1 \;\; u_2 \,]^T,\ Q = 0$ and $R = 2$ resulting in

$$\min_{u_1,u_2} \sqrt{2(u_1^4 + 6u_1^2u_2^2 + u_2^4)} \Leftrightarrow \min_{x_1,x_2} x_1^2 + 6x_1x_2 + x_2^2, \tag{15}$$

where the equivalence follows from the substitution $x_1 = u_1^2, x_2 = u_2^2$. The eigenvalues of the objective Hessian are given by

$$sp(H(x_1^2 + 6x_1x_2 + x_2^2)) = sp\left(2 \begin{bmatrix} 1 & 3 \\ 3 & 1 \end{bmatrix} \right) = \begin{bmatrix} -4 \\ 8 \end{bmatrix}. \tag{16}$$

(The objective is not convex, since its Hessian is indefinite.)

Further, there does generally not exist u_b, which bring the norm of (13) to 0. For instance, if $u_a \neq 0$ and $Q = 0$, this would result in u_b of negative energy.

2.4 Particular Problem

Here, without further motivation, the norm R of (13) was chosen to be a weighted Euclidean norm. The weighting was chosen 1 for elements $j \in I$ corresponding to frequencies ω_j between the two peaks of $|U_{a,180}|$ and $|U_{a,90}|$ and 0 for all other elements. All elements of Q were chosen as $\max_j |(U_a)_j|$, corresponding to the flat energy spectrum in the third quadrant, shown in Fig. 5. For notational convenience, the sequence u_b was chosen to be of the same length as u_a, i.e., $N_a = N_b = N/2$.

2.5 Optimization

We have not found any convexifications of (13), without introducing relaxations resulting in suboptimality. The proposed optimization strategy consists in two iterative stages. During the first stage, the error $J(u_k)$ is monotonically non-increasing in the iterations k. The second stage lacks this property, but has shown good results in all experiments. The solution is chosen as

$$u_k^*,\ k^* = \arg\min_k J(u_k), \tag{17}$$

and is obtained either from the last iteration of stage one or any (usually among the last) iteration of stage two.

Stage One Each iteration of the algorithm consists in sorting the frequencies ω_j, between the $|U_{a,180}|$ and $|U_{a,90}|$ peaks with respect to corresponding magnitude error. Starting with the w_j corresponding to the largest error, a sinusoid Δu_b in phase with the existing w_j component in u is added to u_b. The amplitude is chosen to minimize the norm in (13). If the norm cannot be decreased by $\epsilon = 5\%$, Δu_b is discarded, and the next ω_j from the sorted list is assessed. If the norm cannot be decreased by ϵ for any ω_j, stage one is terminated. Else, a new iteration is executed, now with u replaced by $u + [0 \cdot u_a^T \;\; \Delta u_b^T]^T$.

An algorithmic presentation is given in Algorithm 1. For notational convenience, we introduce

$$\Delta u_{0,b} = [0 \cdot u_a^T \;\; \Delta u_b^T]^T \tag{18}$$

and

$$W_b = \theta(N_a + 1) - \theta(N), \tag{19}$$

where $\theta(k)$ is the Heaviside step at k.

The problem of minimizing J over a is given by

$$\min_a \underbrace{\sum_{j \in I} |Q_j - |F_j(u + a\Delta u_{0,b})|^2|^2}_{M_1(a)}, \tag{20}$$

Algorithm 1 Synthesis of u_b, stage one.

repeat
  flag = false
  queue = $\text{sort}_j\ |Q_j - P_j|$
  for all j in queue **do**
    $\Delta u_{0,b}\ = W_b \text{Ш}_h(t)\cos(\omega_j t + \phi_j)$
    $a\ = \arg\min_j\ J(u + a\Delta u_{0,b})$
    $\Delta u_{0,b} * = a$
    if $J(u + \Delta u_{0,b})/J(u) < 1 - \epsilon$ **then**
      $u\ = u + \Delta u_{0,b}$
      flag = true
    else
      flag = false
      break
    end if
  end for
until not flag

where $M_1(\cdot)$ is a forth order polynomial with known coefficient. Hence the solution of (20) is given by

$$\min_{a\in A} M(a),\ A = \left\{a; \frac{dM_1}{da} = 0\right\}. \tag{21}$$

Fig. 7(a) shows the result, when the algorithm is applied to u from Fig. 6(a). The corresponding power spectrum is shown in Fig. 7(b).

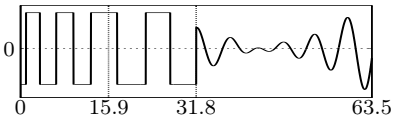

(a) Input u over time [s].

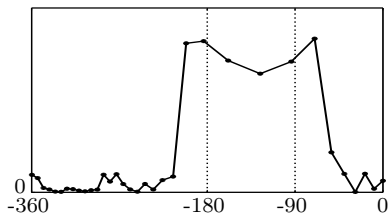

(b) Power spectrum $|U|^2$ over process phase φ [°].

Fig. 7. Input signal and corresponding power spectrum after first optimization stage.

Stage Two This stage is similar to stage one, but rather than minimizing the error norm, the magnitude error at ω_j is brought to 0 in each iteration. Due to spectral leakage, however, the magnitude errors at $\omega_{l\neq j}$ might simultaneously increase. An algorithmic presentation is given in Algorithm 2.

Algorithm 2 Synthesis of u_b, stage two.

repeat
  $j\ = \arg\min_j |Q_j - P_j|$
  $\Delta u_{0,b}\ = W_b \text{Ш}_h(t)\cos(\omega_j t + \phi_j)$
  $a\ = \arg\min_a |Q_j - |F_j(u + a\Delta u_{0,b})|^2|$
  $u\ = u + a\Delta u_{0,b}$
until $|Q_j - P_j| < \epsilon$

The minimization step is similar to that of Stage one, with (20) replaced by

$$\min_a |\underbrace{\sqrt{Q_j} - |F_j(u + a\Delta u_{0,b})|}_{M_2(a)}|, \tag{22}$$

where $M_2(\cdot)$ is a third order polynomial with known coefficients.

Fig. 8(a) and 8(b) correspond to Fig. 7(a) and 7(b). The error $J(u_k)$ over iterations k is shown in log scale in Fig. 9. The vertical line indicates the boundary between stages one and two.

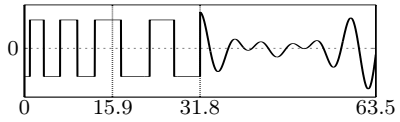

(a) Input u over time [s].

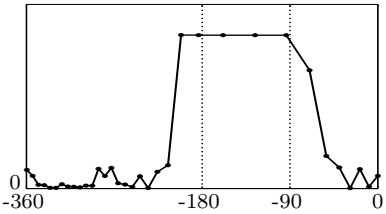

(b) Power spectrum $|U|^2$ over process phase φ [°].

Fig. 8. Input signal and corresponding power spectrum after second optimization stage.

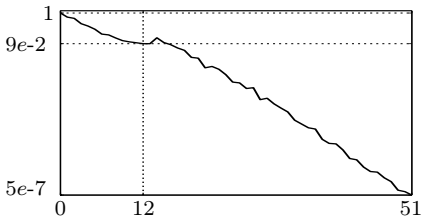

Fig. 9. Normalized error $J(u_k)/J(u_0)$ over optimization iterations k. Vertical line marks boundary between stage one and two. Logarithmic scale.

2.6 Practical Considerations

Limiting Leakage In addition to parametrizing u_b in sinusoids, with phases chosen to be consistent with u, one might consider various windows, to reduce spectral leakage. However, practical experience has shown that windowing does not contribute significantly to the convergence of the presented algorithms.

The amplitude constraint (14) can be incorporated in the algorithms by limiting $|a|$ in each iteration, to a value where the constraints are met. Naturally, this imposes suboptimality. The level of suboptimality can be decreased by increasing the length of u_b, N_b.

Depending on how the signal pair u, y will be used, one may or may not care about the magnitude spectrum outside the reference window. One way of avoiding spectral leakage from the optimization to form peaks at the edges of the window is to begin each optimization iteration by

detecting the largest peak outside the window and add an out of phase sinusoid, reducing it to a tolerable value. This method was used when generating the results, presented below.

Noise and Relay Hysteresis It is not desirable to trigger subsequent relay switches at zero crossings, due to noise. A straight forward method for avoiding this is the introduction of hysteresis, which can be either in the signal magnitude or time domain. Here, signal magnitude is advantageous, since the time scale is unknown a priori.

Adapting the Sample Period Since the experiment duration is unknown a priori, the approach has been to introduce a buffer of fixed length $N_a = 2^{10}$. The system is then sampled with period h_0 (as fast as the hardware allows) until the buffer is filled. The sample period is updated $h_1 = 2h_0$ and every second sample is overwritten, corresponding to a down sampling of a factor 2. If the experiment is not completed when the end of the buffer is reached anew, the procedure is repeated with $h_{k+1} = 2h_k$.

Meeting the Real-Time Constraint Since the optimization needs to be conducted online, it starts executing at the second last switch of u_a in Fig. 6(a). Stage one is associated with a halting criterion, while stage two executes until the last switch of u_a. The time between the second last and last switch is assumed to be the same as that between the third and second last.

3. SIMULATION RESULTS

The algorithms described above have been evaluated on a large set of FOTD and SOTD processes of the forms

$$P_1(s) = \frac{e^{-s}}{1+sT_1},\ P_2(s) = \frac{e^{-s}}{(1+sT_1)(1+sT_2)}, \qquad (23)$$

with varying $T_k, k = 1, 2$ corresponding to normalized time delay in the range $0.17 < \tau < 0.98$.

Fig. 10 shows the power spectra (cf. Fig. 8(b)) resulting from applying the method to the batch. The spectra have been normalized w.r.t. Q in (13), to facilitate visualization. Algorithm 2 was limited to run $k_{\max} = 100$ iterations.

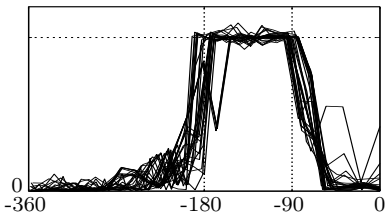

Fig. 10. Power spectra $|U|^2$ over process phase φ [°] for a FOTD and SOTD batch.

4. PHYSICAL EXAMPLE

Once the input has been applied to the system, the recorded input and output data is used to fit a FOTD or SOTD model. This is done in two stages. The first stage consists in obtaining initial parameters and deciding model order, using a vector-fitting approach, under current development. The second stage is a gradient based optimization, described in Soltesz et al. [2010], minimizing

$$J(\theta) = \frac{1}{2}\int_{t_0}^{t_f} [y(t) - \hat{y}_\theta(t)]^2 dt, \qquad (24)$$

where y is the recorded output and $\hat{y}_\theta$ the output of a simulation using a transfer function parametrized in θ.

Once the model is obtained, it is used as the basis for choosing PID parameters. The method of choice is one by Garpinger and Hägglund [2008], where the integrated absolute error (IAE) from a load step disturbance is minimized, subject to sensitivity, complementary sensitivity and control signal variance constraints, as outlined in (25). Cf. Fig. 2, where C is the transfer function of the PID controller.

$$\begin{aligned} &\min_{K,T_i,T_d \in \mathbb{R}^+} \int_0^\infty |e(t)|dt \qquad (25)\\ &\text{s.t.}\\ &|S(i\omega)| \le M_s, |T(i\omega)| \le M_t, \forall \omega \in \mathbb{R}^+,\\ &||C(s)S(s)||_2^2 = \frac{\sigma_u^2}{\sigma_n^2} \le V_k. \end{aligned}$$

Without going into further detail regarding the two last blocks of Fig. 1, the operation of the auto-tuner is demonstrated, using a lab scale tank process. A schematic sketch is shown in Fig. 11(a). Fig. 11(b) shows a photo of the actual process.

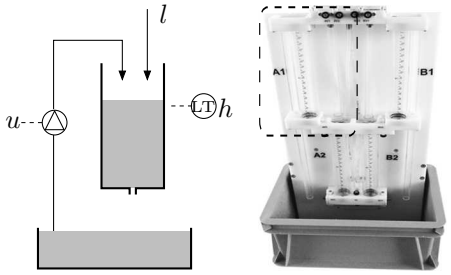

(a) Schematic sketch. (b) Photograph.

Fig. 11. Tank process. Dashed region in photo marks sketch.

First principle modeling, Bernoulli [1738], yields the ODE

$$\frac{dh}{dt} = -\frac{a}{A}\sqrt{2gh} + \alpha u, \qquad (26)$$

where h [m] is the (measured) water level, $u \in (0, 1)$ is the input, proportional to the inflow through α [$\mathrm{m}^3{\cdot}\mathrm{s}^{-1}$]. l [$\mathrm{m}^3{\cdot}\mathrm{s}^{-1}$] is an uncontrolled and unmeasured disturbance flow. A, a [m^2] are the tank and outlet cross sections, respectively. The delay L [s] is due to the actuating pump and (intentionally) slow communications.

Linearizing around a nominal level h_0 [m] and introducing $y = \beta h \in (0, 1)$, where β [m^{-1}] is the sensor gain, an FOTD model is obtained:

$$\Delta Y(s) = \frac{Ke^{-sL}}{sT+1}\Delta U(s),\ K = \frac{\alpha}{a}\sqrt{\frac{2x_0\beta}{g}},\ T = \frac{A}{a}\sqrt{\frac{2x_0}{g\beta}}. \qquad (27)$$

The Δ:s denote deviation from the linearization point. Note however that the available signals are u, y rather

than $\Delta u, \Delta y$. Also note that only non-negative inflow is possible, i.e., $\alpha = 0$ when $u < 0$.

Fig. 12(a) shows the input signal generated by the proposed method together with that of a traditional relay experiment. The signals are of equal duration and energy. The corresponding power spectra are shown in Fig. 12(b). Here process phase is that obtained when inserting numerical measurement values of $a,\ A,\ \alpha,\ \beta,\ h_0,\ L$ into (27).

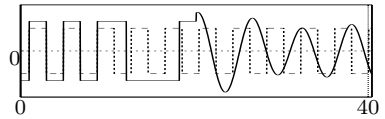

(a) Input signal u_a over time [s].

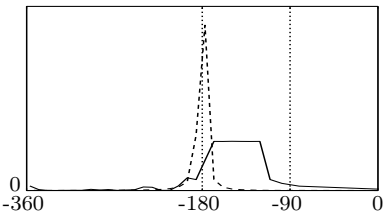

(b) Power spectrum $|U_a'|^2$ over process phase φ [°].

Fig. 12. Input signal and corresponding power spectrum from tank experiment. Relay (dashed), extended (solid).

From Fig. 12(a) it is obvious that fitting the three FOTD parameters to the input-output data of the traditional relay comes with numerical difficulty, since virtually all energy is concentrated to a narrow spectral peak, yielding only one complex number, i.e., two parameters.

Based on the input-output data from the extended relay experiment, PI parameters were obtained using Garpinger and Hägglund [2008] with $M_s = M_t = 1.4$, $V_k = 4$. Fig. 13(a) shows the plant output of experiments where a reference step from $r = 0.8h_0$ to h_0 occurred at $t = 5$ s, followed by a load step at $t = 30$ s. At $t = 70$ s, white zero mean measurement noise, with variance 0.005, was added. Fig. 13(b) shows the corresponding u.

5. CONCLUSION

The paper addresses the problem of input magnitude spectrum shaping, in the context of PID auto-tuning.

A two stage optimization method, for magnitude spectrum shaping was presented and demonstrated. It shows satisfactory result for the class of processes (FOTD and SOTD) interesting from a PID tuning perspective.

The algorithm was applied to physical data and the autotuning procedure, of which the algorithm is a part, was outlined and demonstrated.

6. FUTURE WORK

A natural question is if the problem formulation (13) can be relaxed into a convex program (without introducing suboptimality). It is also of interest to see if this can be done when the second part, u_b, of the input is constrained according to (14), which defines a convex region.

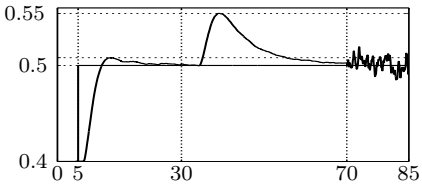

(a) Ref. r and output y over time [s].

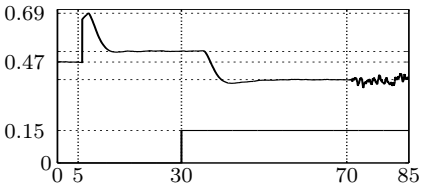

(b) Input u and load l over time [s].

Fig. 13. Closed loop response to reference step, load step and measurement noise. (There is a 5 s transport delay on the disturbance step, due to the hardware.)

From a signal generation perspective it would be even more beneficial if u_b was only allowed to take binary values $\in \{u_{\min}, u_{\max}\}$, as is the case for u_a. This results in a binary program of high dimensionality, which is not tractable without further reformulation or relaxation.

It is desirable to choose magnitude $||u_a||_\infty$, resulting in $c_l \cdot \sigma_n < ||y_a||_\infty < c_h \sigma_n$, where σ_n is the standard deviation of the output y_a due to measurement noise. $c_l \approx 1$ and $c_2 \approx 2$ are constants. This is a feedback problem, since the process gain is unknown before the experiment.

In addition, several issues concerning the two rightmost blocks in Fig. 1, remain to be addressed before the PID tuning chain functions reliably enough for industrial use.

REFERENCES

Karl Johan Åström and Tore Hägglund. Automatic tuning of simple regulators with specifications on phase and amplitude margins. *Automatica*, 20:645–651, 1984.

Karl Johan Åström and Tore Hägglund. *Advanced PID Control*. ISA, 2006. ISBN 1-55617-942-1.

Karl Johan Åström, G C Goodwin, and P R Kumar. *Adaptive Control, Filtering and Signal Processing*. Springer-Verlag, 1995. ISBN 0-387-97988-3.

Daniel Bernoulli. *Hydrodynamica*. 1738.

Mats Friman and Kurt V. Waller. A two-channel relay for autotuning. *Industrial and Engineering Chemistry Research*, 36:2662–2671, 1997.

Olof Garpinger and Tore Hägglund. A software tool for robust PID design. In *Proc. 17th IFAC World Congress, Seoul, Korea*, July 2008.

Tore Hägglund and Karl Johan Åström. Revisiting the Ziegler-Nichols tuning rules for PI control. *Asian Journal of Control*, 4(4):364–380, December 2002.

Chong Lin, Qing-Guo Wang, and Tong Heng Lee. Relay feedback: A complete analysis for first-order systems. *Industrial and Engineering Chemistry Research*, 43:8400–8402, 2004.

Kristian Soltesz, Karl Johan Åström, and Tore Hägglund. Transfer function parameter identification by modified relay feedback. *American Control Conference, Proceedings of*, 2010.